Measurements of Magnetic Field of Variable Period Undulator and Correction of Field Errors

Yaroslav Gorbachev[1, a)], Igor Davidyuk[1], Stanislav Serednyakov[1], Nikolay Vinokurov[1], Vladimir Tcheskidov[1], Anton Pavlenko[1], Alexandr Batrakov[1], Konstantin Shtro[1] and Oleg Shevchenko[1, b)]

[1] Budker Institute of Nuclear Physics SB RAS,
pr. Akad. Lavrent'eva 11, , 630090, Novosibirsk, Russia

[a)]Corresponding author: jiva-5m@yandex.ru
[b)] O.A.Shevchenko@inp.nsk.su

Abstract. A new variable period undulator of unique design was developed and built recently at Budker INP. It will replace the electromagnetic undulator in use now on the second FEL of the Novosibirsk FEL facility. As a result, the FEL tunability range will be substantially extended. In this paper, we present the results of measurements of the undulator magnetic field for different periods and discuss ways to reduce the field errors, which include sorting of magnets, weakening of undulator edge poles, and using of steering coils.

INTRODUCTION

The concept of the variable period undulator (VPU) was proposed several years ago [1]. The main advantage of such undulator as compared with conventional design undulators with similar parameters is its wider radiation wavelength tunability range. Usually the wavelength in an undulator is tuned by variation of the magnetic field amplitude. In this approach, to obtain a shorter wavelength one should significantly reduce the field amplitude, which leads to reduction in the spontaneous emission intensity or FEL gain. The VPU design can be optimized so that the field amplitude remains relatively large for short wavelengths.

There are several ways to vary the undulator period. Recently, a VPU with a very simple mechanical design was proposed and built at Budker INP [2,3]. It utilizes repulsive forces that act between adjacent magnet units. This undulator will replace the electromagnetic undulator in use now on the second FEL of the Novosibirsk FEL facility [4] (see Fig. 1).

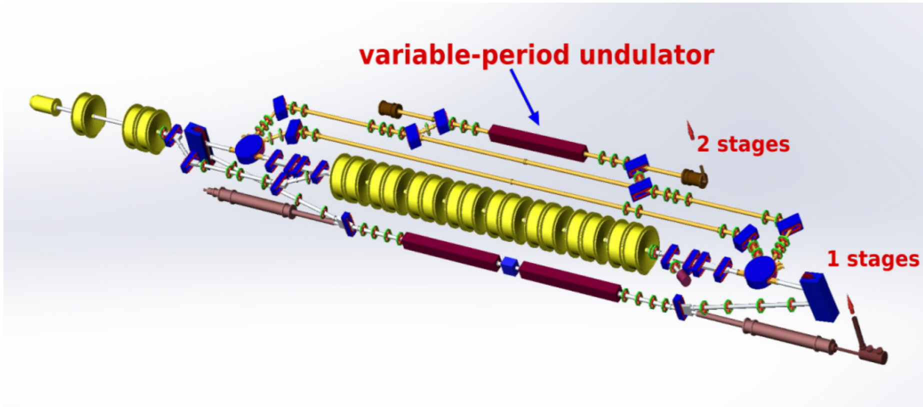

FIGURE 1. Layout of Novosibirsk FEL facility (top view). Beamlines of 3rd FEL are not shown.

After this upgrade, the current FEL tunability range of 35 – 80 μm will be extended to 15 – 80 μm. Another unique feature of the new undulator design is that it allows changing the number of periods. Parameters of the old electromagnetic (EM) and new (VP) undulators are compared in Table 1.

TABLE 1. Comparison of electromagnetic and variable period undulator parameters.

Parameter	EM	VPU
Undulator period λ_w, mm	120	48 – 96
Aperture (diameter of inscribed circle), mm	70	50
Number of periods	33	30 – 80
Field amplitude, kGs	0 – 1.3	1 – 1.9
Deflection parameter K	0 – 1.55	0.45 – 2
Undulator length, m	4	4
Radiation wavelength, μm	35 – 80	15 – 80

The FEL gain strongly depends on the undulator field quality, which has to be controlled and improved during magnetic measurements. A standard set of quality improvement methods includes sorting of magnets before undulator assembling, as well as compensation of the field first and second integrals. In the case of VPU, there are also some specific procedures to ensure uniform longitudinal distribution of magnet units.

The new NovoFEL undulator has already been assembled. We controlled and sorted all the magnets and almost finished the measurements of magnetic field. The results of these measurements are presented in this paper.

UNDULATOR DESIGN

The mechanical design of the VPU includes the aluminum frame with guiding grooves, in which movable cassettes with magnets (magnet units) are installed. Smooth moving of the cassette along the undulator axis is achieved by installing bearings on the cassette housing, which fit into the grooves of the undulator frame. Each magnet block consists of one magnet and two iron plates adjacent to the magnet from two sides perpendicular to the undulator axis. One such plate corresponds to one halve of the undulator pole. One unit includes two magnet blocks and an aluminum cassette, and they move as a whole (see Fig. 2). The left and right magnet blocks of the unit are placed symmetrically and inclined with respect to each other. This geometry ensures increase in the vertical magnetic field amplitude in both the vertical and horizontal directions. As a result, the undulator will focus the electron beam horizontally and vertically. It should be noted that the undulator focusing is strong in our case because of low beam energy. The two units located above and below the undulator plane of symmetry move independently, but the strong attractive force acting between them holds them together. Thus, the undulator aperture takes the form of a rhombus with an inscribed circle diameter of 50 mm, as shown in Fig. 2.

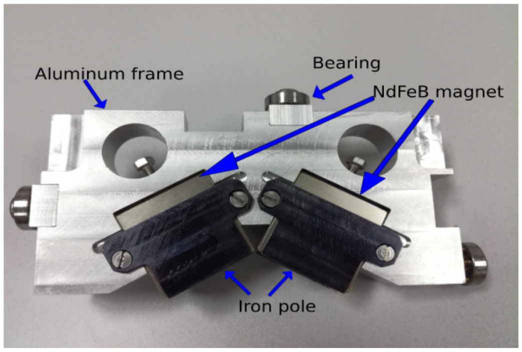

(a)

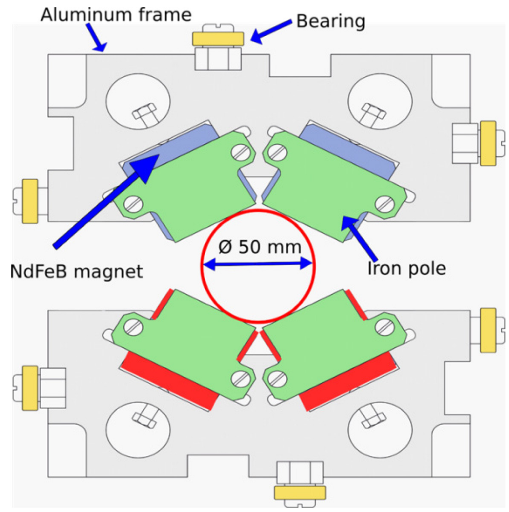

(b)

FIGURE 2. (a) Assembled magnet unit and (b) arrangement of units in undulator.

In the undulator design under consideration, only the positions of the end magnet units are fixed. The inner units can move freely in the longitudinal direction, but strong repulsive forces arising between adjacent units automatically distribute them uniformly. The undulator period is varied by shifting the end units with the help of pushers installed outside on the undulator frame. The pushers are driven by stepper motors with reduction gears (see Fig. 3).

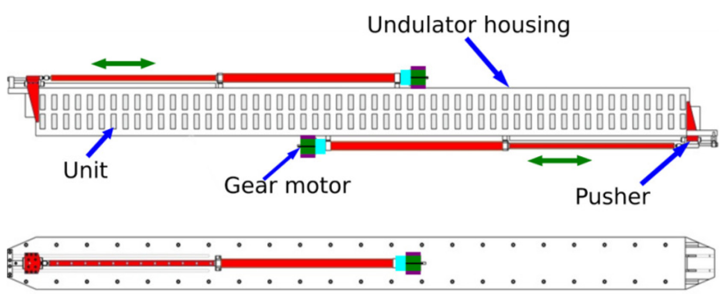

FIGURE 3. Undulator frame with all units installed. Pushers are used to adjust undulator period.

SORTING OF MAGNETS AND ASSEMBLING THE MAGNET UNITS

The magnet production process does not provide the magnetization tolerance required in undulators. The standard solution of this problem is sorting of magnets. To make the sorting one should measure all components of magnetization for each magnet that is planned to be used in undulator. The measurement procedure can be organized the following way. Suppose that we have a magnet placed in the magnetic field created by a solenoid with a fixed current. If we move this magnet to infinity, where the solenoid magnetic field vanishes, then the magnetic field energy changes according to the following expression [5]:

$$\Delta E = \int \left(\vec{M} \cdot \vec{B}\right) dV = I \int \varepsilon\left(t\right) dt\,, \tag{1}$$

where $\vec{M}$ is the magnetization vector, $\vec{B}$ is the solenoid magnetic field, I is the solenoid current, and $\varepsilon(t) = -\frac{1}{c}\frac{\partial\Phi}{\partial t}$ is the emf induced in the solenoid. The volume integral is taken over the magnet. If the solenoid magnetic field can be taken to be uniform within the magnet with only one component directed along the axis Z, then we get the following expression for the magnetization component averaged over the magnet body:

$$\langle M_z \rangle = \frac{1}{V_0}\frac{I}{B_z}\int \varepsilon(t)\, dt, \tag{2}$$

where V_0 is the magnet volume and the ratio of the solenoid current to its field is some constant. One can see from (2) that the averaged magnetization is proportional to the integral over time of the emf induced in the solenoid during the magnet removal.

In our undulator we use NdFeB magnets with dimensions of 40x40x20 mm. The layout of the setup for sorting the magnets is shown in Fig. 4. The solenoid is composed of three coaxially arranged radial coils. The two outer coils are identical and the third coil with reduced number of turns is placed between them. Due to this design, in the center of the solenoid there is a region with a uniform magnetic field. Each magnet is uniquely placed in the center of the coil and then removed a large distance. The signal induced in the solenoid is measured by the integrator VsDC3, developed at Budker INP [6]; then it is processed by the computer code and saved into a file.

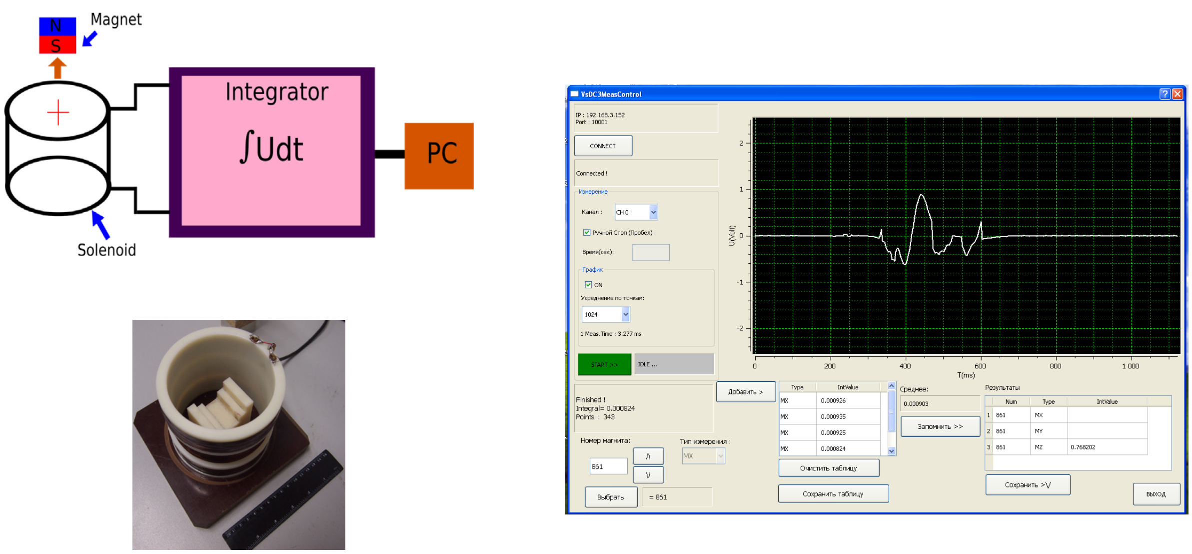

(a) (b)

FIGURE 4. (a) Layout of setup for sorting magnets and (b) example of measurement.

All the three magnetization components were measured for all magnets. The distribution of the main magnetization component error normalized to its mean value is shown in Fig. 5. As a result of sorting, we have chosen 570 magnets from 953. The final distribution is shown in green. The final standard deviation of the normalized magnetization error is $2.1\cdot10^{-3}$, which satisfies our requirements.

After sorting, the magnets were installed to cassettes. This procedure was not quite trivial because of strong forces acting between magnets. To make this work, a special jig was designed, which prevented the magnets from sticking together (see Fig. 6a).

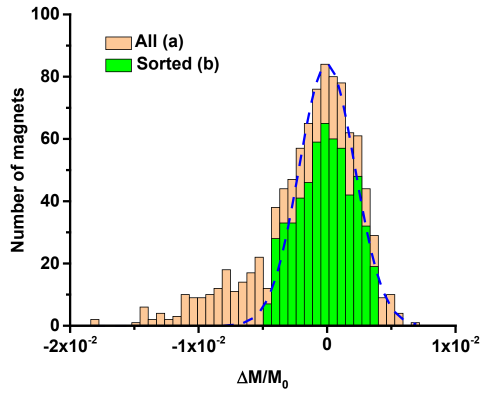

FIGURE 5. Distribution of magnetization for all and sorted magnets.
Gaussian distribution with $\sigma = 2.2 \cdot 10^{-3}$ is plotted by dashed curve for reference.

Due to safety requirements, we also needed a special storage system for assembled magnet units. A special box was developed, into which the cassettes were inserted sideways in one row at a fixed distance from each other. Due to the attraction forces, the cassettes are securely fixed in their cells. The cassettes can be inserted from the front and from the back of the box. One box holds 10 cassettes on each side. The boxes can be conveniently stored stacked one on another (see Fig. 6 b).

(a) (b)

FIGURE 6. (a) Setup for installing magnets to cassettes and (b) cassette storage system.

MEASUREMENT OF THE MAGNETIC FIELD

Magnetic measurement setup

To measure the undulator magnetic field, a special setup was developed (see Fig. 7). In this setup, a stepper motor pulls a toothed belt with a carriage mounted on it in a special rail on the undulator axis. Such scheme enables measurements with an increment of 0.1 mm and positioning accuracy of ± 0.05 mm. To map the undulator magnetic field, we used a carriage with five Hall sensors HE144 [7] with a spacing of 7.5 mm. The voltage measurement by the sensors and the movement of the carriage are handled by a specialized magnetic measurement system, based on equipment in the VME standard [8] and modernized to use the HE144 sensor. The sensors mounted on the carriage were calibrated in a magnet with a uniform field using an NMR magnetometer, which is part of the system [9]. The zero-bias voltage for each channel is determined in a magnetic screen before each measurement and is taken into account by the software. The measurement error in the range of undulator field values does not exceed ± 0.2 Gs.

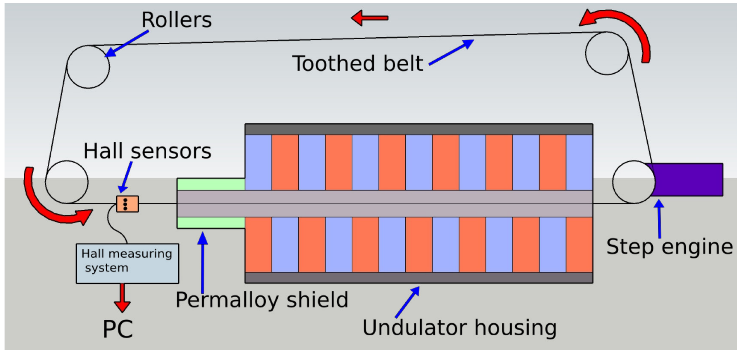

FIGURE 7. Layout of magnetic measurement setup.

Undulator field measurement results

Undulator magnetic field was measured for different undulator periods and for different number of poles. Some basic undulator parameters obtained for the regular part of the measured field are presented in Fig. 8. The radiation wavelength is calculated assuming an electron energy of 22 MeV. The measured undulator parameters agree very well with the results of simulations [3].

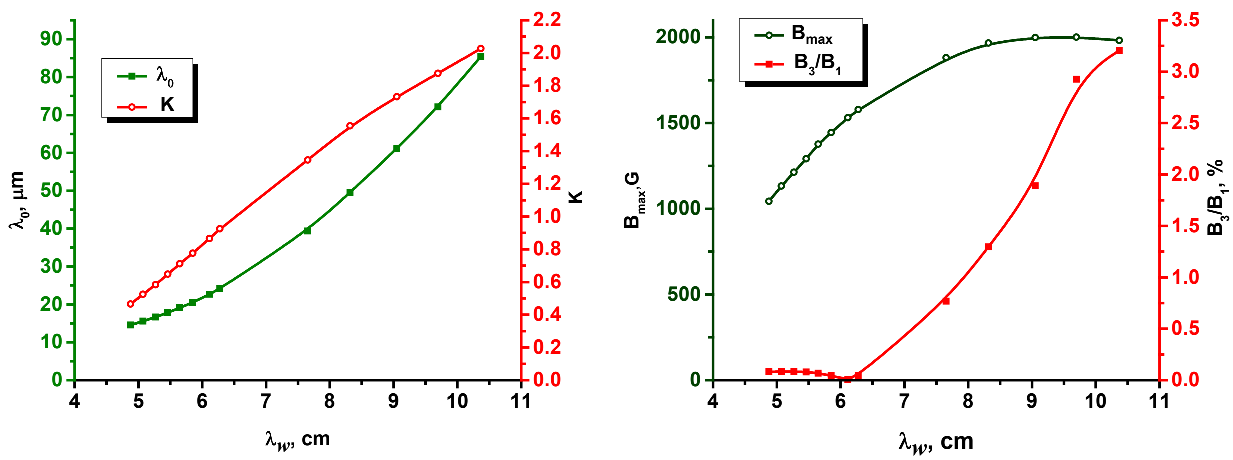

(a) (b)

FIGURE 8. Basic undulator parameters for different periods: (a) radiation wavelength for electron energy of 22 MeV and undulator deflection parameter, (b) maximum magnetic field and 3[d] harmonic.

Figure 9 illustrates the dependence of the magnetic field 1[st] harmonic amplitude on the transverse coordinate in the undulator median plane for an undulator period of 10.4 cm. Increase in the amplitude from the undulator axis leads to beam focusing in the horizontal direction. The second plot in Fig. 9 shows dependence of matched beta functions on the undulator period.

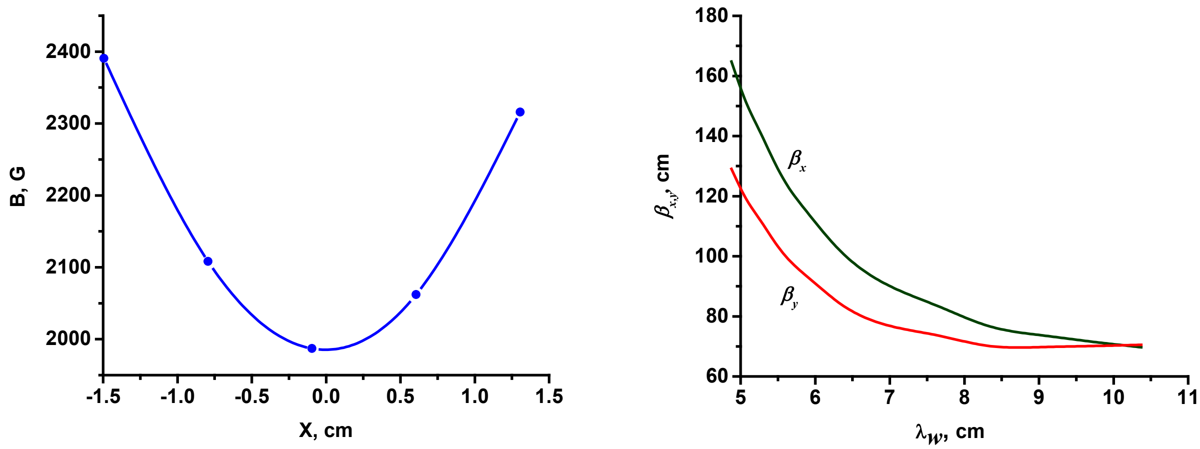

(a) (b)

FIGURE 9. (a) Dependence of 1st harmonic amplitude on transverse horizontal coordinate (λ_w = 10.4 cm) and (b) dependence of matched beta-functions on undulator period.

FRINGE FIELDS AND FIELD ERROR COMPENSATION

The magnet sorting procedure reduced the field errors in the regular part of the undulator to permissible limits. But there are some sorts of errors that cannot be eliminated this way. To ensure that electrons are moving along the undulator axis, one must compensate the first and second integrals of the magnetic field. The tolerance requirement for this compensation is determined by the radiation mode transverse size (for our case it is about 2 mm). The fields to correct for this compensation are the undulator fringe fields and external scattered fields. One way to correct the fringe field is to reduce the magnetization of the end units' magnets.

The magnetization can be reduced by heating the magnets. The Curie point for NdFeB magnets is 310-340 °C; after this temperature magnets lose their magnetization. Weakening of magnetization with increasing temperature near the Curie point occurs nonlinearly, which complicates the choice of heating regime. To determine the dependence of magnetization on heating temperature, we made a series of experiments. To heat magnets we used a muffle furnace. The magnets were placed in the cold furnace and when the required temperature was reached, the furnace was turned off and left to cool for a day. The temperature was controlled using a chromel-alumel thermocouple. After that, the magnetization at room temperature was measured. The results are shown in Fig. 10.

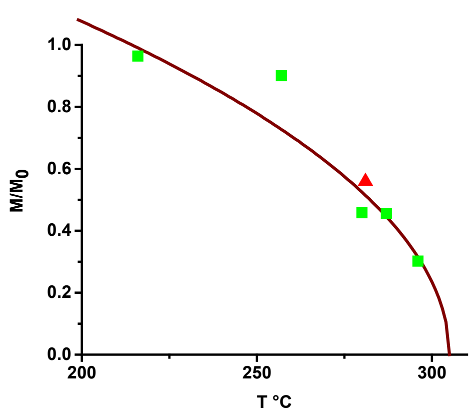

FIGURE 10. Dependence of magnetization reduction on magnet heating temperature.

For the fringe field correction, the magnetization of the end unit magnets was reduced two-fold. To achieve this reduction, the magnets were heated up to 281 °C. To correct the external scattered field (which is mainly the Earth field), we use a distributed steering coil. It can create a weak vertical magnetic field of up to 1.5 Gs. The coil has six turns made of copper wire with a cross-section area of 1.5 mm^2. The coil is fixed directly to the undulator frame by a U-shaped aluminum profile. The working current of the coil is 10 A. The field correction methods applied substantially reduced the field integrals , as shown in Fig. 11.

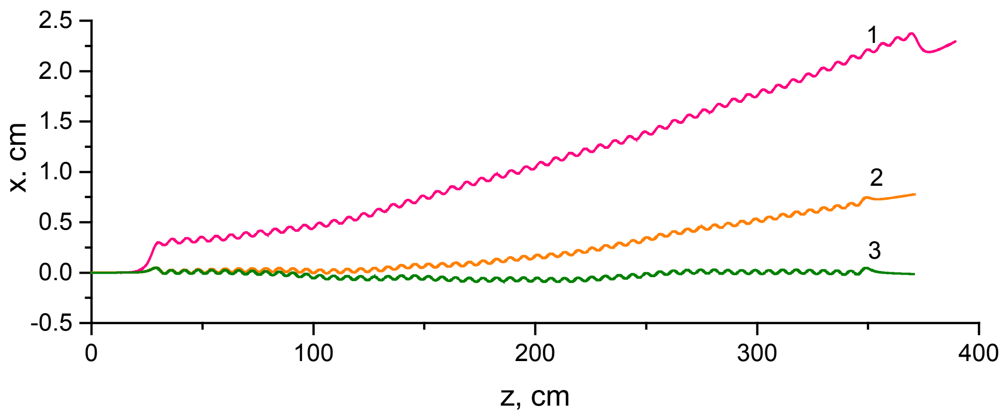

FIGURE 11. Reference particle trajectory: 1- no compensations; 2 – undulator fringe field is corrected; 3 – external scattered field is corrected. Particle energy is 22 MeV; undulator focusing is not taken into account.

UNDULATOR FIELD QUALITY CONTROL BY THE RADIATION SPECTRA

It is known that the FEL gain at small signal approximation is proportional to the frequency derivative of the electron spontaneous emission spectrum in the direction of the undulator axis [10]. One can use this spectrum to evaluate the undulator magnetic field quality. For a given particle trajectory, the Fourier transform of the vector potential can be determined from the following expression [11]:

$$A_{x\omega} = \frac{q}{c}\frac{e^{ikR_0}}{R_0}\int_{-\infty}^{\infty} v_x(t)\, e^{i(\omega t - kz(t))}dt = \frac{q}{c}\frac{e^{ikR_0}}{R_0}\int_{z_{in}}^{z_{out}} x'(z)\, e^{i\omega(t(z)-z/c)}dz\,, \tag{3}$$

where R_0 is the distance from some point in the undulator to the observation point, q is the particle charge, $x'(z)$ is the particle velocity angle with respect to the undulator axis, $t(z) \approx t(z_{in}) + \frac{1}{v_0}\left(z - z_{in} + \frac{1}{2}\int_{z_{in}}^{z} x'^2(\tilde{z})\,d\tilde{z}\right)$ is the moment of time when the particle arrives at the coordinate z (v_0 is the particle velocity), and z_{in} and z_{out} are the longitudinal coordinates of some points before and after undulator where the undulator field vanishes. Here we assume that R_0 is much larger than the undulator length. The energy emitted by the particle to the frequency range $d\omega$ and solid angle $d\Omega$ is equal to [11]

$$dE = \frac{c}{2\pi}k^2\left|A_{x\omega}\right|^2 R_0^2\, d\Omega \frac{d\omega}{2\pi}. \tag{4}$$

One can see that the desired spectral distribution is determined by the integral in (3), which can be written in the following form:

$$J\left(\kappa\right)=\int_{z_{in}}^{z_{out}}\gamma x'\left(z\right)\exp\left\{i\kappa\left[\int_{z_{in}}^{z}\gamma^2 x'^2\left(\tilde{z}\right)d\tilde{z}-z+z_{in}\right]\right\}dz \quad (5)$$

where $\kappa = k/\left(2\gamma^2\right)$.

The squared module of (5) normalized to the ideal undulator case for different undulator periods and different number of periods is shown in Fig. 12.

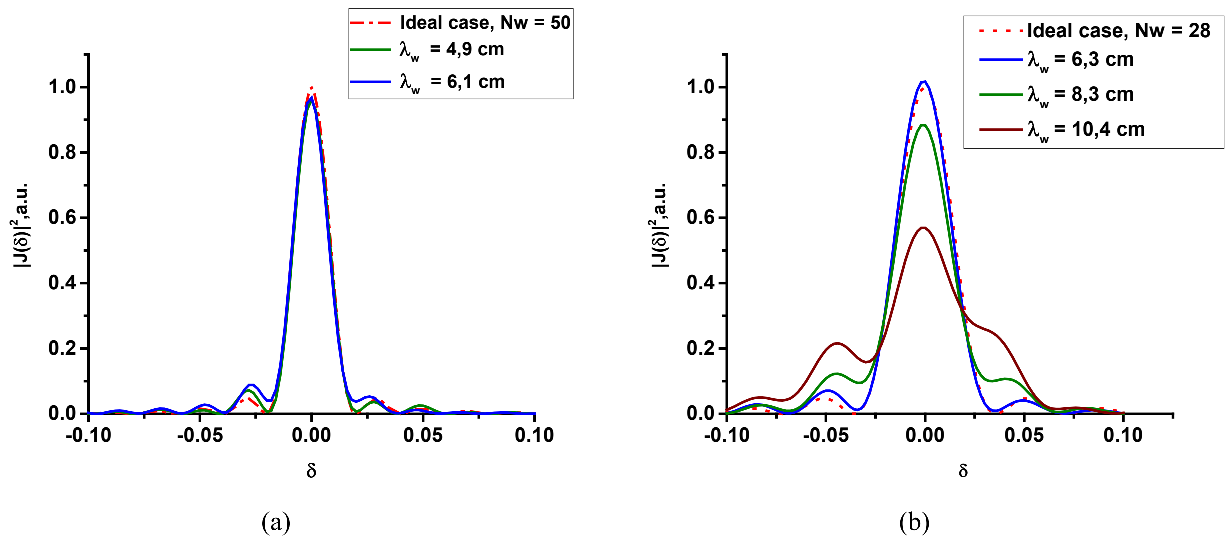

FIGURE 12. Normalized radiation spectra for different undulator periods and different number of poles: (a) 106 poles; (b) 60 poles. Here $\delta = \left(\kappa - \kappa_0\right)/\kappa_0$, and κ0 is position of maximum of $|J|^2$.

As it can be seen from Fig. 12, in the case of small undulator periods, the radiation spectra almost perfectly coincide with the ideal undulator spectrum that has slightly (by 2-3) fewer periods. The strong degradation of the spectrum for a large undulator period can be explained the following way. Repulsive forces acting between adjacent units become weaker when the distance between the units increases and the influence of friction forces becomes significant. The units are not distributed uniformly anymore; their distribution now depends on the history of their motion. This effect can be observed in the magnetic field measurement results. The unit centers are located very close to the points where the field becomes zero, and coordinates of the zero field points can be easily determined (see Fig. 13).

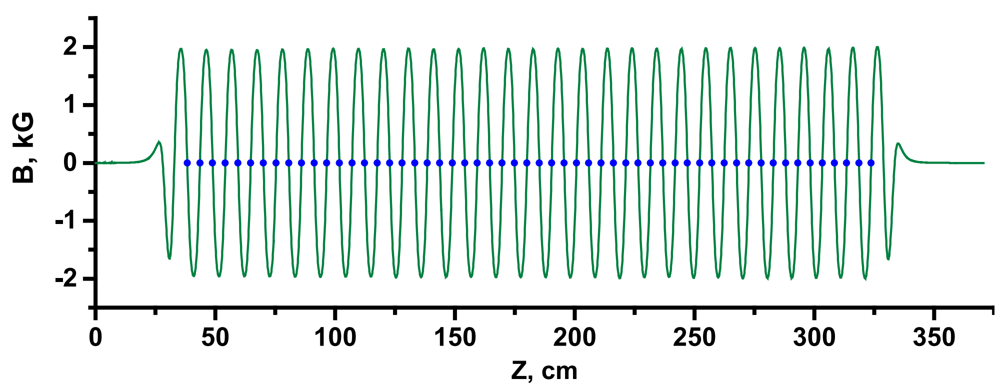

FIGURE 13. Longitudinal positions of magnet units for case of maximum undulator period.

The plots in Fig. 14 show how the distance between adjacent units changes with the unit number for different undulator periods. One can see that for large periods, the distance is not constant; it changes linearly from the beginning to the end of undulator, which explains the radiation spectrum broadening.

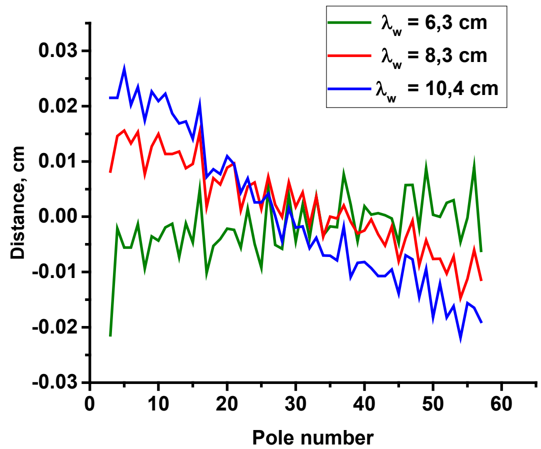

FIGURE 14. Distance between adjacent poles vs. pole number.

To avoid this effect and get uniform distribution of the magnet units at large undulator periods one has to use slightly more sophisticated algorithms of period adjustment, which are planned to be tested.

CONCLUSION

Magnetic measurements of the new NovoFEL undulator are almost finished. The field quality is sufficient for the FEL operation. Most of the field errors were corrected. Some procedures to ensure uniformity of the magnetic unit distribution must be tested yet. The undulator is planned to be installed on the second FEL of the NovoFEL facility in the nearest future.

REFERENCES

1. G.K. Shenoy, J.W. Lewellen, D. Shu, and N.A. Vinokurov, J. Synchrotron Radiat. **10**, 205 (2003).
2. N.A. Vinokurov, O.A. Shevchenko, V.G. Tcheskidov, in *Proc. FEL2010* (Malmö, Sweden, 2010), p. 696.
3. I. Davidyuk, O.A. Shevchenko, V.G. Tcheskidov, and N.A. Vinokurov, Phys. Rev. Accel. Beams **19**, 020701 (2016).
4. O.A. Shevchenko, N.A. Vinokurov *et al*., Bull. Russ. Acad. Sci. Phys. **83**, 228 (2019).
5. L D Landau and E.M. Lifshitz, *Electrodynamics of Continuous Media* (Butterworth-Heinemann, 1984), pp. 113–121.
6. A. Batrakov, A. Pavlenko, D. Shickov, and P. Vagin, Proceedings of RuPAC 2012, Russia, pp. 617-619.
7. Datasheet Analog Hall Sensor HE144. URL: https://www.asensor.eu/onewebmedia/Datasheet-HE144X.pdf.
8. The New VME-based system for magnetic measurements with Hall sensors. A.Batrakov, S.Zverev, I.Ilyin, V.Kozak, E.Kuper, V.Mamkin, V.Ovchar, G.Fatkin, V.Tsukanov, P.Vobly, A.Volkov. Preprint/ Budker INP 2007-32, Novosibirsk, 2007, Russia.
9. PRECISE MAGNETOMETERS ON BASE OF PULSED NMR TECHNIQUES. G.V.Karpov, A.S.Medvedko, E.I.Shubin. Proceedings of RuPAC 2006, Novosibirsk, Russia. p. 58-60.
10. J. M. J. Madey, Nuovo Cimento B **50** 64 (1979)
11. L D Landau and E.M. Lifshitz, *The Classical Theory of Fields* (Butterworth-Heinemann, 1987), pp. 159–170.